PERGAMON

Atmospheric Environment 36 (2002) 4173–4187

ATMOSPHERIC ENVIRONMENT

www.elsevier.com/locate/atmosenv

A simulation of long-range transport of Yellow Sand observed in April 1998 in Korea

Hee-Jin In, Soon-Ung Park*

School of Earth and Environmental Sciences, Seoul National University, San 56-1 Shilim-Dong, Kwanak-Ku, Seoul, 151-742 South Korea

Received 17 December 2001; accepted 27 May 2002

Abstract

A severe Yellow Sand event was observed in Korea for the period of 14–22 April in 1998. The case was reported as a very long lasted event and transported to the western part of USA across the Pacific Ocean. This event was simulated using a three-dimensional eulerian air quality model with MM5 output of meteorological fields. There were large dust rises on 15 and 19 April in the source regions of inland China. These emitted dusts had different transport pathways. The modeled spatial distribution of dust was similar to that of aerosol index obtained by total ozone mapping spectrometer. The simulated dust concentration was slightly underestimated the observed total suspended particulate concentration in South Korea. However, the arriving time of the dust storm to the Korean Peninsula was quite well simulated. The simulated particle sizes in Korea were found to be less than 6–7 μm in diameter with a uni-modal size distribution at a peak dust concentration in the range of 1.73–4.03 μm during the Yellow Sand event. These results suggest that the present model can be used to forecast the Yellow Sand event in South Korea.

Keywords: Dust emission; Particle size distribution; MM5 model; TOMS aerosol index; Eulerian air quality model

1. Introduction

Yellow Sand, which is a typical example of mineral aerosol frequently originates in the Sand desert, the Gobi desert and Loess plateau in China during the spring season. The source regions of Yellow Sand are characterized by dry soil and low vegetation covers. Dusts can be uplifted into the middle troposphere by strong surface winds in the source regions and have a diameter ranging from 0.1 to about 1000 μm. Large particles with a diameter greater 30 μm settle down near the source region, while relatively small particles have a lifetime of several days to weeks and can be transported up to several thousand kilometers (Zhang and Carmichael, 1999). The particles having a diameter of 1–16 μm with an average of 4 μm are known to be long-range transported aerosols over Korea, Japan, and sometimes even over the Pacific Ocean (Hanna et al., 1999).

A severe Yellow Sand event was observed in Korea for the period of 14–22 April in 1998. This case was reported as a very long lasted event and dusts emitted in China have been transported across the Pacific Ocean to the west coast of USA (Husar et al., 2001; Chun et al., 2001; Uno et al., 2001; Park and Chang, 2000). Park and Chang (2000) simulated long-range transport of this event using the tracer continuity equation. In their study, starting and ending times of the Yellow Sand event observed in Korea were quite well simulated. However, dry and wet deposition processes and the particle size classification were not considered in their model. Yoon and Won (1998) monitored aerosols in Seoul during this Yellow Sand event and analyzed the aerosol size, number concentration and extinction coefficient for this chosen case. The results indicated that the total suspended particulate (TSP) concentration during the Yellow Sand event was about 3 times higher

*Corresponding author. Tel./fax: +82-2-880-6715.
E-mail address: supark@snupbl.snu.ac.kr (S.-U. Park).

1352-2310/02/$ - see front matter
PII: S1352-2310(02)00361-8

than that of the non-Yellow Sand period with a significant increase in particle diameter of 3–7.2 μm. The sulfate and nitrate concentrations also significantly increased.

The purpose of this study is to develop an aerosol model including processes of emission, transport, dry and wet deposition of particles that can simulate long-range transport of Yellow Sand observed during 14–22 April 1998 in Korea to understand important mechanisms of long-range transport of the Asian dust.

2. Model description

2.1. The meteorological model

The meteorological model used in this study is the fifth-generation mesoscale model of non-hydrostatic version (MM5, Pennsylvania State University/National Center for Atmospheric Research) defined in the x, y and σ coordinate. The equation sets of MM5 are primitive physical equations of momentum, thermodynamics and moisture. The state variables are temperature, specific humidity, wind component and pressure (Grell et al., 1994; Dudhia et al., 1998). Four physical processes including the cloud cooling scheme for radiation, the Kain–Fritsch scheme for convective parameterization, the Blackadar scheme for planetary boundary layer processes and the mixed phase (Reisner) for moisture explicit schemes are used.

The domain of the model is shown in Fig. 1. The domain includes major source regions of Yellow Sand: the Sand, Loess and Gobi (Chun, 1966). The model has 112×86 grids having a horizontal resolution of 39 km with 21 vertical layers (σ values of each layer are 1.000, 0.995, 0.990, 0.985, 0.98, 0.97, 0.96, 0.945, 0.93, 0.91, 0.89, 0.865, 0.84, 0.78, 0.7, 0.6, 0.5, 0.4, 0.3, 0.2, 0.1, and 0). The simulation covers the period from the first dust-rise report in the source region on 13 April to the end of the Yellow Sand event observed in Korea on 22 April 1998.

2.2. Aerosol transport model

The aerosol model includes physical processes such as three-dimensional advection, diffusion, dry and wet depositions. Transforming the general aerosol equation to the σ coordinate system (Westphal et al., 1987) is

$$\frac{\partial p_* C(r)}{\partial t} = -\frac{\partial p_* C(r) u}{\partial x} - \frac{\partial p_* C(r) v}{\partial y} - \frac{\partial}{\partial \sigma} C(r)(p_* \dot{\sigma} + g\rho V_f) + p_* \frac{\partial}{\partial x} K_h \rho \frac{\partial C(r)/\rho}{\partial x} + p_* \frac{\partial}{\partial y} K_h \rho \frac{\partial C(r)/\rho}{\partial y} + \frac{g^2}{p_*} \frac{\partial}{\partial x} K_z \rho^3 \frac{\partial C(r)/\rho}{\partial x} + p_* C_0 + p_* S, \quad (1)$$

where $C(r)$ is the concentration of spherical particles of radius r, u and v the horizontal winds, V_f the fall velocity (positive downward), $p_* = P_{surf} - P_{top}$, ρ the air density, g the gravitational acceleration, K_h the horizontal eddy diffusivity, K_z the vertical eddy diffusivity, C_0 the coagulation term and S the source and sink. Coagulation is not included in simulations because it is not an important process in the evolution of dust outbreaks (Westphal et al., 1987, 1988).

The second-order Bott scheme for the advection calculation is used to minimize the numerical diffusion term (Bott, 1989). The surface and boundary layer similarity theory are used for the parameterization of eddy diffusivity for the different stability regime (Businger et al., 1971). The deposition processes of particles are included in this model. Dry deposition uses the inferential method (Wesely et al., 1985; Wesely, 1989) with taking into account the gravitational settling velocity while wet deposition follows the RADM model (Chang et al., 1987, 1991).

Model domain, horizontal grid spacing and vertical layers in σ coordinate are the same as those of MM5 model. Hourly meteorological variables obtained from the MM5 run are feed to the transport model. To solve the equation numerically the operator-splitting technique (Chang et al., 1987) is applied. Individual terms in Eq. (1) are independently computed in parallel for short time periods. Generally integral time steps of each term are different.

2.2.1. Dust source strength

The method for the estimation of dust emission amounts ranging 0.1–30 μm in radius is given as:

$$F_a = \left\{ \sum_i (1 - f_i R_i) \right\} \times 5.2 \times 10^{-14} u_*^4 \quad \text{if } u_* \geqslant u_{*t}, \quad (2)$$

where F_a is the dust flux from the surface ($g\,cm^{-2}\,s^{-1}$), u_* the friction velocity, u_{*t} the threshold friction velocity, f_i the fractional coverage of i type of vegetation in dust source grid and R_i the reduction factor of i type of vegetation (In and Park, 2002; Westphal et al., 1987; Gillette, 1981). Twenty-four different land use types are identified from the advanced very high resolution radiometer (AVHRR) in the source region. The threshold friction velocities are found to be 60, 50, and 40 $cm\,s^{-1}$ in Gobi, Sand and Loess region (In and Park, 2002).

Particles of 0.1–30 μm in radius are divided into 10 size bins with the same logarithm intervals in Table 1. Total emission amounts are apportioned to each bin using a power law with a factor of 1.5, namely,

$$\frac{dF}{d \log r} \propto r^{1.5}, \quad (3)$$

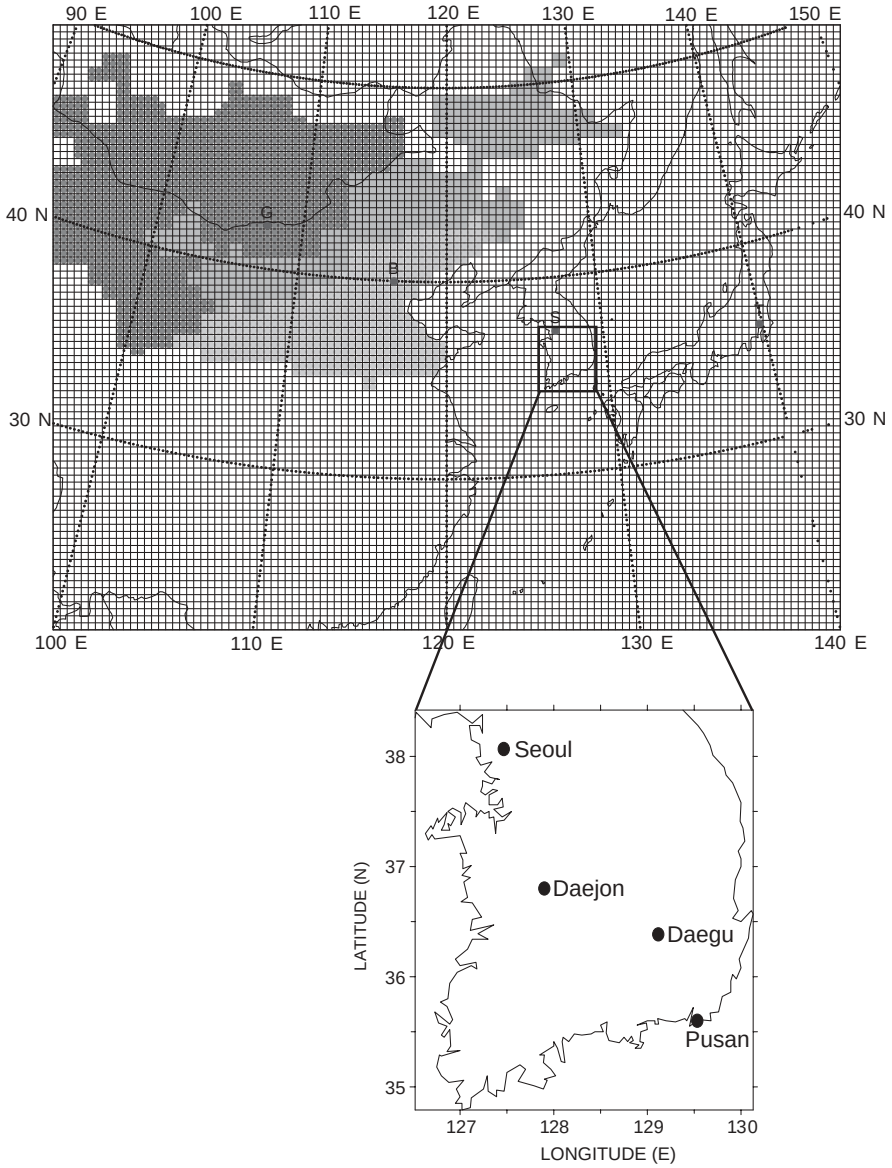

Fig. 1. The model domain and the Yellow Sand source region in a $39 \times 39\,km^2$ grid scheme. The marks (◆), (■) and (●) represent the Gobi, Sand and Loess regions. The lettered dot marks indicate the locations of a Gobi site (G), Beijing (B), Seoul (S), and Tokyo (T). The locations of 4 cities in South Korea are also shown.

where r is the particle radius (Westphal et al., 1987; Chung, 1996; Schûtz and Jaenicke, 1974).

2.2.2. Initial and boundary conditions

The dust concentrations of each size bin are given initially zero. For the treatment of boundary concentrations, a positive-definite zero-flux outflow boundary condition with an appropriate flow divergence restriction is used. That is

$$u_1(C_1 - C_0)/\Delta x = u_2(C_2 - C_1)/\Delta x \quad (4)$$

gives

$$C_0 = \max\left\{0, C_1 - \frac{u_2}{u_1}(C_2 - C_1)\right\}, \quad (5)$$

where C_0, C_1 and C_2 represent concentrations outside the domain, at the boundary cell and first cell of the inner domain, respectively. u_1 is the wind at the outer boundary flux point and u_2 the wind at the inner boundary flux point. When u_1 is sufficiently small (smaller than $10^{-3}\,m\,s^{-1}$) or the wind is divergent at

Table 1
Particle size divisions

Bin number	Range of particle radius (μm)	Mid radius (μm)
1	0.10–0.18	0.13
2	0.18–0.31	0.24
3	0.31–0.55	0.42
4	0.55–0.98	0.74
5	0.98–1.73	1.30
6	1.73–3.06	2.30
7	3.06–5.42	4.08
8	5.42–9.59	7.21
9	9.59–16.96	12.75
10	16.96–30.00	22.56

the boundary cell ($u_1 \times u_2 < 0$), a zero concentration gradient at the outflow boundary ($C_0 = C_1$) is imposed.

3. Overviews of the chosen Yellow Sand event

3.1. Synoptic conditions of the chosen Yellow Sand event

Fig. 2 shows the 00 UTC surface weather charts at 00 UTC on 15 and 19 April 1998. A surface low-pressure system was located at 50°N and 115°E with a cold front extended through Mongolia at 00 UTC 15 April. Over the northwestern and southwestern parts of the low-pressure center, high-pressure centers were located. Strong winds exceeding $10\,m\,s^{-1}$ prevailed between the high- and low-pressure systems with large horizontal pressure gradients. As the low-pressure system moved eastward, there were dust rise reports behind the cold front over the sand desert and Loess areas. This low-pressure system kept to move eastward being elongated southward. Behind the surface low-pressure system over the Loess and Sand desert at the southeastern border of Mongolia and China, a large amount of dust rise was reported and then continuously moved southeastward.

At 00 UTC 19 April, a new low-pressure system was located at southeastern Mongolia. This low-pressure system moved rapidly northeastward to reach Manchuria next day. Dusts were continuously raised for two days (19–20 April) at the behind of the cold front associated with the low-pressure system.

3.2. Aerosol index of Total Ozone Mapping Spectrometer (TOMS)

Fig. 3 shows the spatial distribution of aerosol index produced by Total Ozone Mapping Spectrometer (TOMS) during 14–22 April. On 14 April, high value of aerosol index greater than 1 is shown in the Loess region near the Shandong Peninsula and the western part of Korean Peninsula (Fig. 3a). Another aerosol layer appears at the sand desert near the border of eastern Mongolia and China on 15 April (not shown here). Thereafter, it moves southeastward to Central and Eastern China and merges with a dust layer appeared in Manchuria yielding a long band of dust layer on 16 April (Fig. 3b). Thereafter, it progressively moves eastward to the Korean Peninsula and Kyushu of Japan for next two days. The aerosol layer in Eastern China on 18 April (Fig. 3c) moves eastward to locate over Korea on 19 April (not shown here). On 19 April, a new dust layer occurred in Northern China moves eastward to merge with the dust layer in Manchuria on 20 April (Fig. 3d), thereafter, continuously transported eastward to near 40°N while forming a narrow horizontal band (Fig. 3e and f).

3.3. Variations of the TSP concentration observed in Korea

TSP concentrations observed at several monitoring sites (Fig. 1) in Korea on April 1998 are given in Fig. 4. Some of the TSP concentrations in Fig. 4 are averaged values of nearest several sites. The maximum concentration of TSP during the Yellow Sand event is 3–6 times higher than the monthly mean value of $35–90\,\mu g\,m^{-3}$ in most sites. The observed TSP concentration in Seoul (Fig. 4a) does not increase for the first 5 days after the Yellow Sand event being reported. However, it starts to increase from 18 April to reach a maximum of $220\,\mu g\,m^{-3}$ on 20 April. Thereafter, it slowly decreases until the end of the Yellow Sand event. However in Pusan, two peak values of TSP concentration occur before ($420\,\mu g\,m^{-3}$) and after the time of maximum concentration in Seoul. TSP concentrations decrease significantly when the precipitation occurs.

4. Results

4.1. Spatial distributions of dust

The spatial distributions of the vertically integrated daily mean dust concentration with the wind vectors at the height of 1500 m ($\sigma = 0.82$) are shown in Fig. 5. A large amount of dusts emitted in Mongolia on 13 April merges with dusts emitted in the Sand and Loess region on 14–15 April (Fig. 5a). The dust laden air moves southeastward continuously following the movement of a trough until 18 April. The trough is elongated through southern China on 16 April and becomes a cut-off vortex over the Yellow Sea on 17 April. The progression of the cut-off vortex drives the movement of dust layer (Uno et al., 2001). On 16 April, dust-laden air in southern China moves counter-clockwise in association with the low-pressure vortex (Fig. 5b) and approaches to

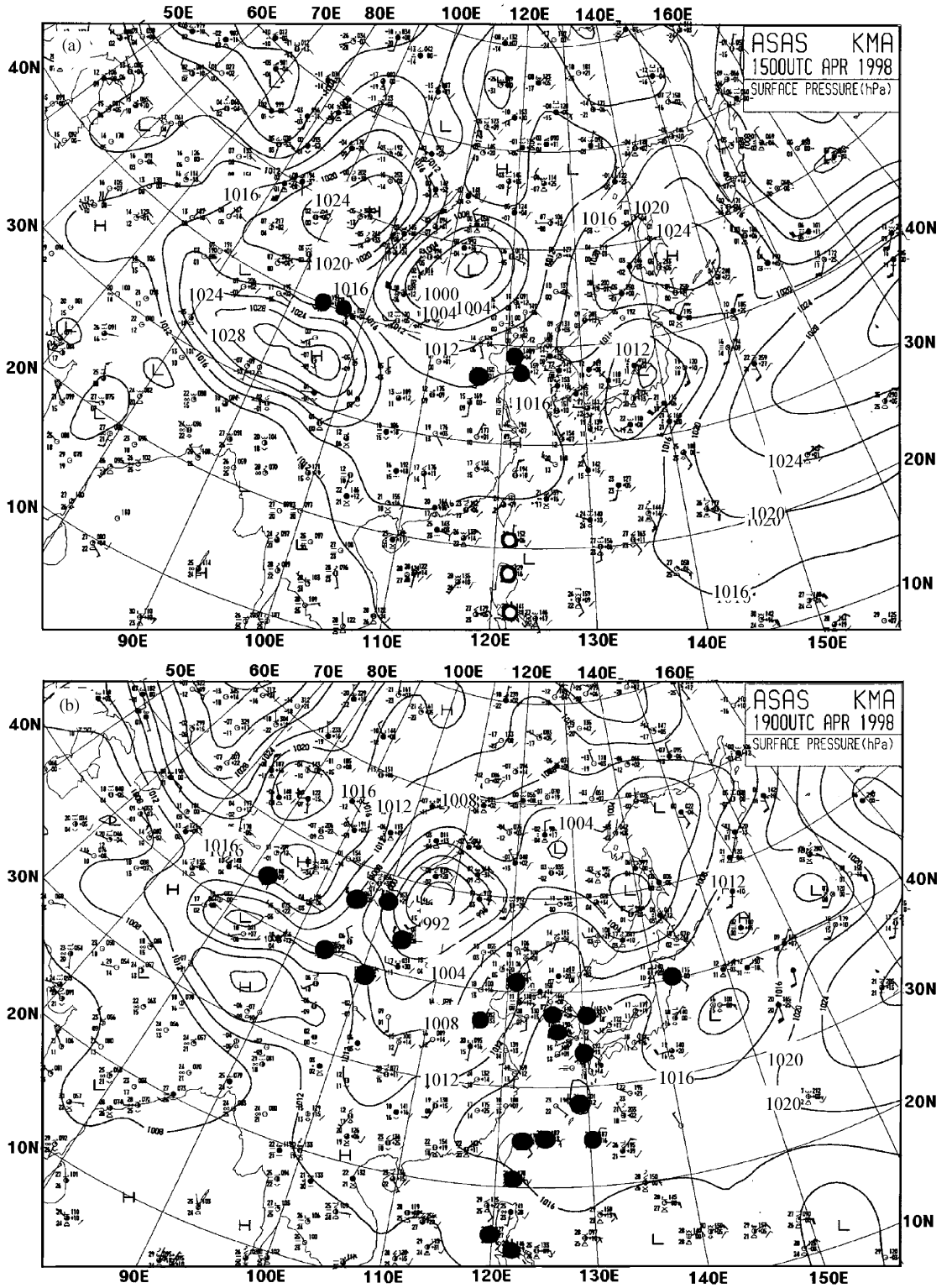

Fig. 2. The surface weather maps at 00 UTC (a) 15 April, (b) 19 April of 1998. The black circle shows sites where the blowing dust or the dust emission is reported.

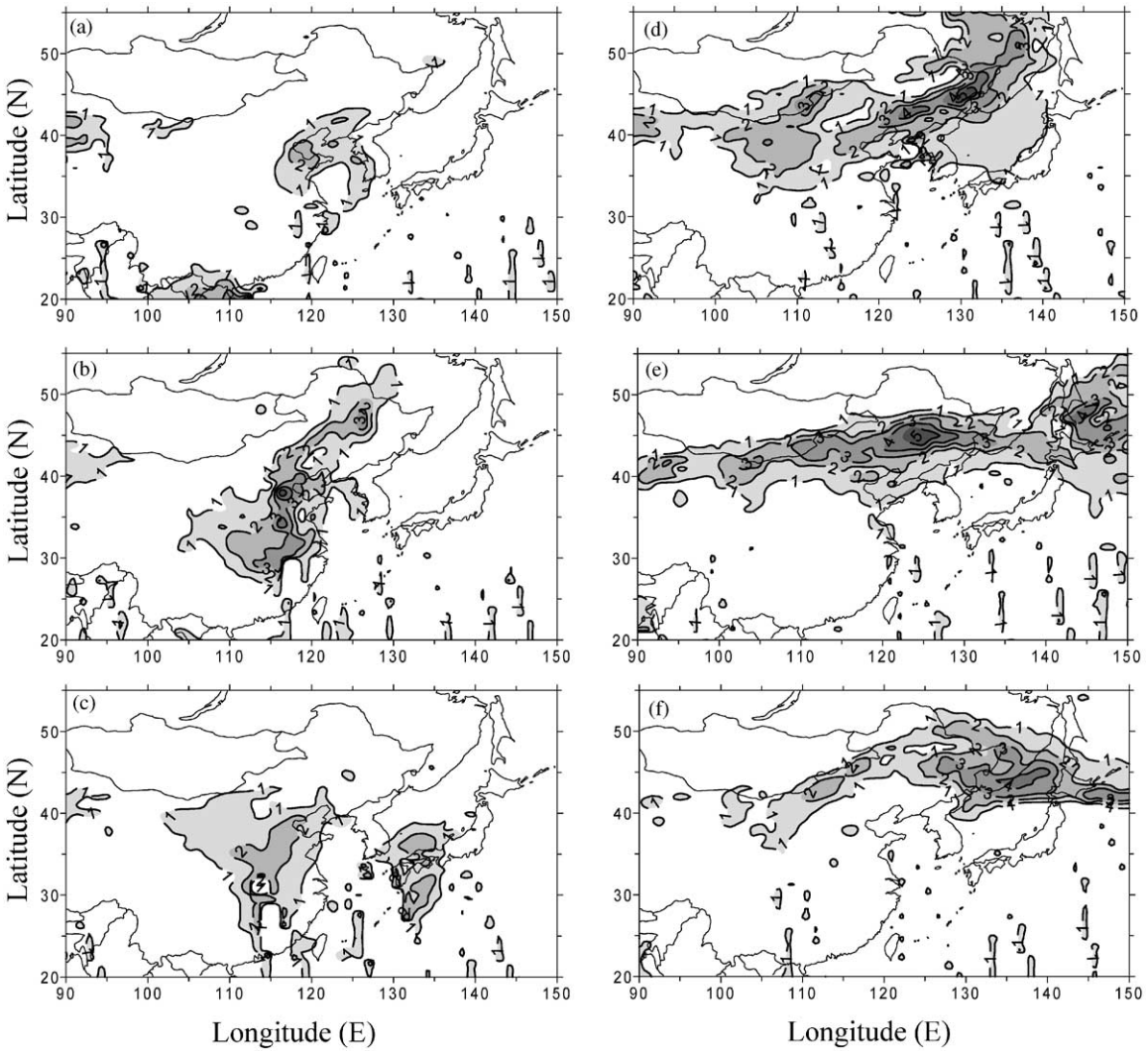

Fig. 3. Aerosol index obtained by TOMS on (a) 14 April, (b) 16 April, (c) 18 April, (d) 20 April, (e) 21 April and (f) 22 April 1998.

South Korea and the southern part of Japan on 17 April. Thereafter, it passes over Japan on 18 April (Fig. 5c). While a dense dust layer appears in Manchuria and Inner Mongolia. On 19 April, the dust layer over Manchuria moves southeastward through the Korean Peninsula and the East Sea. In the meanwhile, a new dust storm developed in northern China moves continuously eastward along 45°N latitude line on 20–22 April (Fig. 5d–f). After 20 April the dust-laden air over the Korean Peninsula and Japan moves northward due to prevailing southerly winds.

Comparing this distribution with the aerosol index in Fig. 3, the model simulates quite well the evolution of dust emitted in the source region except that the emission in Mongolia on 14 and 18 April is somewhat overestimated but the dust layer over the Shandong Peninsula on 14 April is slightly underestimated.

4.2. Longitude-height cross section of TSP concentration

Fig. 6 shows the longitude-height cross sections of the dust concentration and $u - w$ wind vector constructed at near 40°N with a time interval of 12 h from 12 UTC 13 April to 00 UTC 17 April. Vertical winds are exaggerated in order to notify the vertical motion clearly. Dust emitted in the source region ($\sim$115 E) at 06 UTC 13 April (not shown) is transported upward by the upward motion and forms a dust cloud layer whose vertical axis is tilting eastward with height due to high wind speed aloft at 12 UTC 13 April. At this time the upward motion at around 95–100°E is able to raise the dust layer up to 4 km height. The weak horizontal wind and downward motion in the zone of 105–120°E until 00 UTC 14 April confine the dust layer near the source region of 100–105°E. A large amount of dust

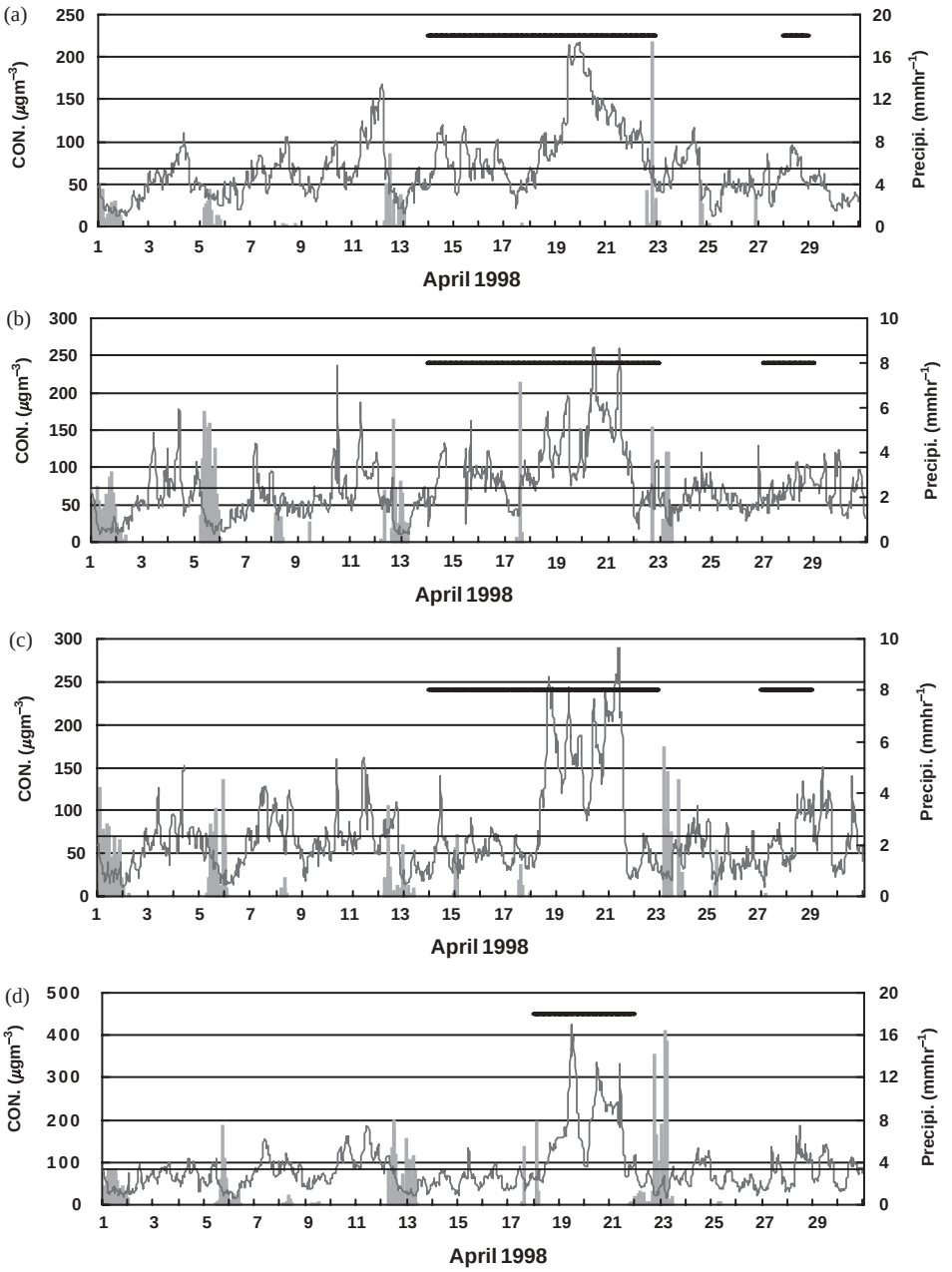

Fig. 4. The TSP concentration (—), Precipitation rate (–) and Yellow Sand Report period (▬) observed at (a) Seoul, (b) Daejon, (c) Daegu, and (d) Pusan in Korea in April of 1998. The horizontal straight line denotes the monthly mean value of TSP concentration for April of 1998.

emitted from 00 UTC to 12 UTC 15 April in the zone of 100–115°E is transported upward to 6 km height as advecting eastward. Since the wind is increasing with height the dust layer is tilted eastward with height. As time progresses the front of dust layer is deepening in the horizontal convergence zone (Fig. 6g and h) while the lowering behind the dust front due to the large scale sinking motion in association with the high-pressure system behind the trough. It is worthwhile to note the overhanged dust layer in front of the dust layer along the propagation direction.

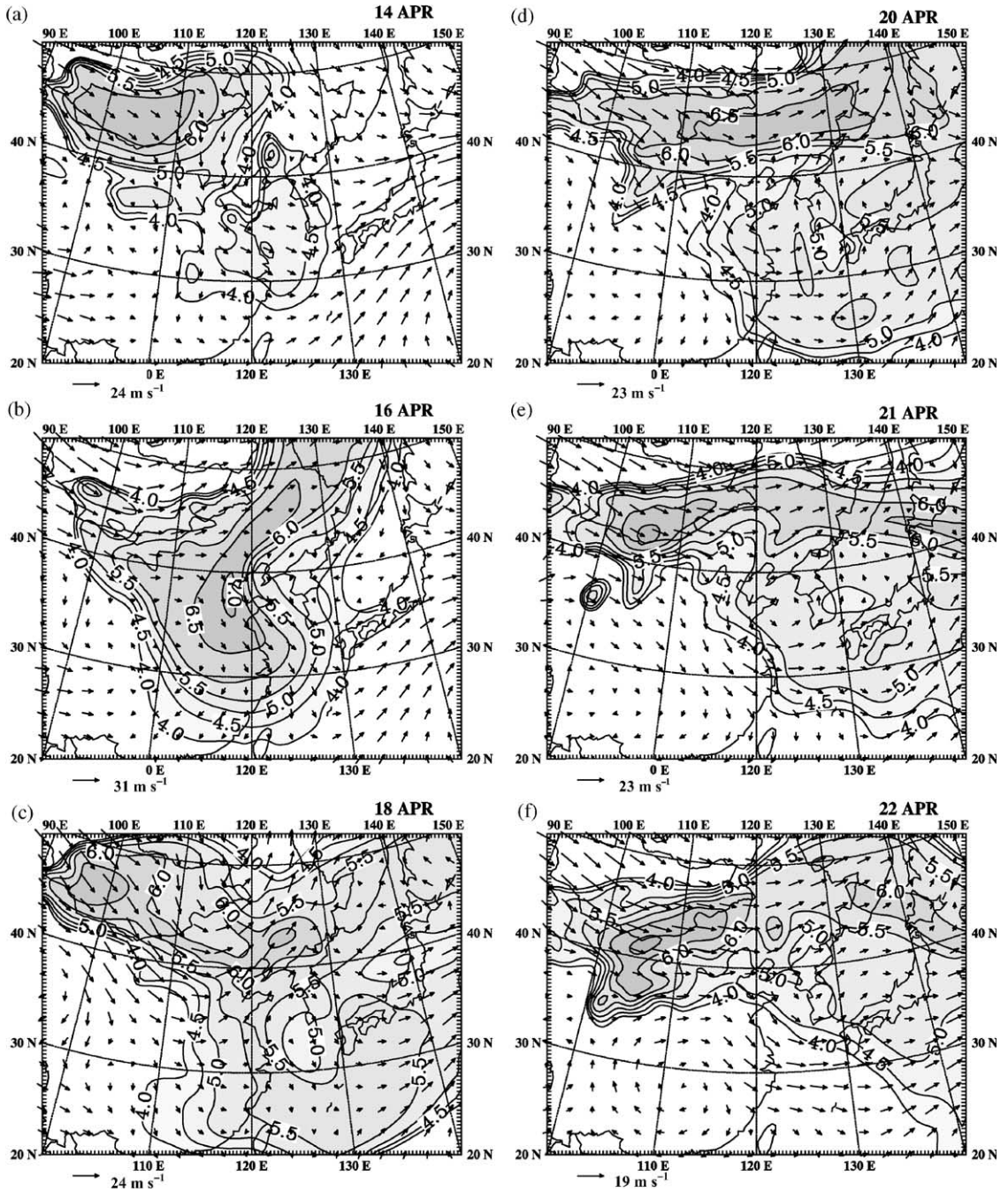

Fig. 5. The same as in Fig. 3 except for the vertically integrated daily mean TSP concentration expressed in common logarithm ($\mu g\,m^{-2}$) with the wind vectors at the height of 1500 m.

4.3. Time-height cross sections of dust concentration at several locations

Fig. 7 shows the time–height cross section of dust concentration with the potential temperature at several locations indicated in Fig. 1. At a site located at the Gobi site (Fig. 7a) high dust concentrations near the surface on 15, 17, 19, and 22–23 April are associated with emissions from the surface. The emitted dusts are uplifted to 4 km above the ground in the mixed layer where the vertical eddy diffusivity is considerably large. During the night the dust layer is mainly confined within

2 km above the ground due to low-level strong stability. Usually, the source regions are located at the height of 1–2 km above the mean sea level but the topographical height decreases eastward. When a mixed layer developed over higher terrain is advected to the lower terrain, an elevated mixed layer is possibly formed if a cold stream or vertical wind shear exists in the low level (Lanicci and Warner, 1991). The development of an elevated mixed layer and the associated circulation (Stensrud, 1993; Keyser and Carlson, 1984) make the dust layer to suspend above 6 km height away from the source region (Chung, 1996). Upward motions caused by synoptic weather systems also promote dusts to move higher layer.

Away from the dust source regions including Beijing (Fig. 7b), Seoul (Fig. 7c), and Tokyo (Fig. 7d), the dust concentration increases in the upper layer first and then the maximum concentration layer moves progressively downward to reach the surface for 1–2 days later. The upward motions caused by the passage

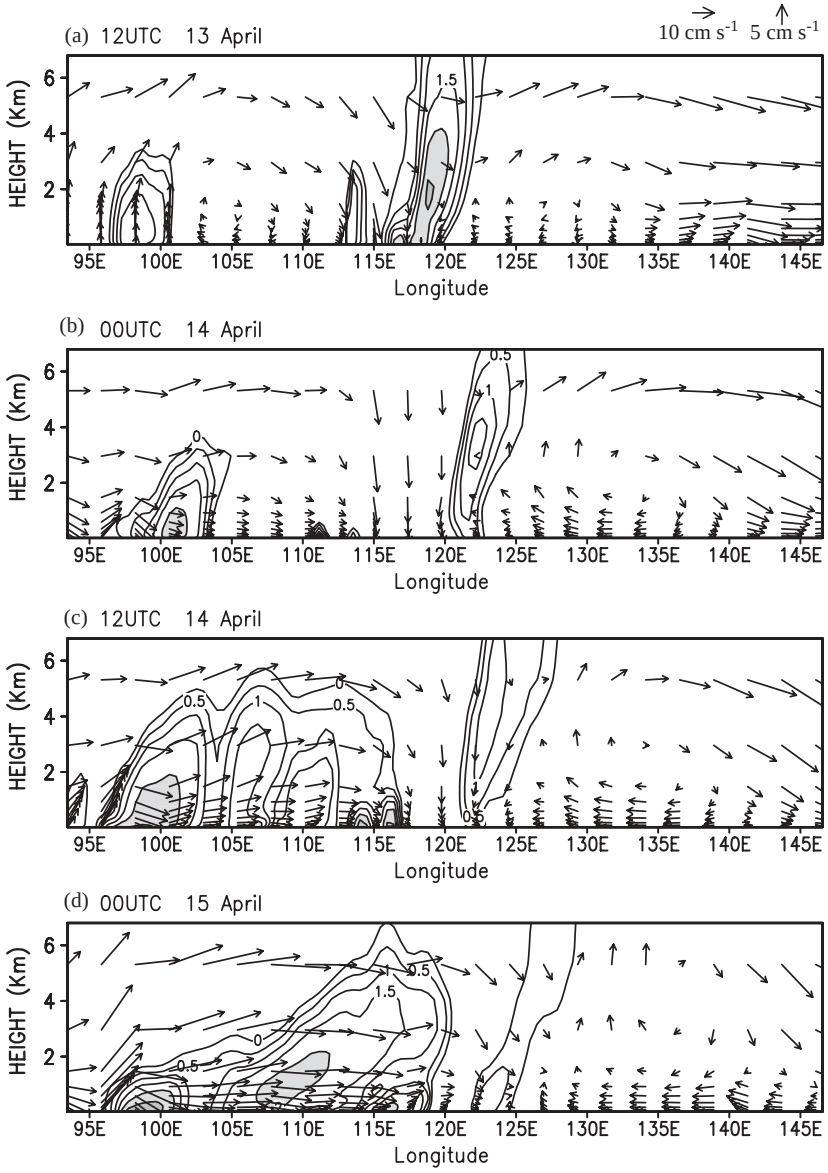

Fig. 6. The longitude-height cross sections of dust concentration (—, power of 10 μg m^{-3}) and $u-w$ wind vector constructed at near 40°N from 12UTC 13 April to 00 UTC 17 April at the time interval of 12 h. The marks ⇧, ⇩ indicate the location of dust layer deeping and sinking.

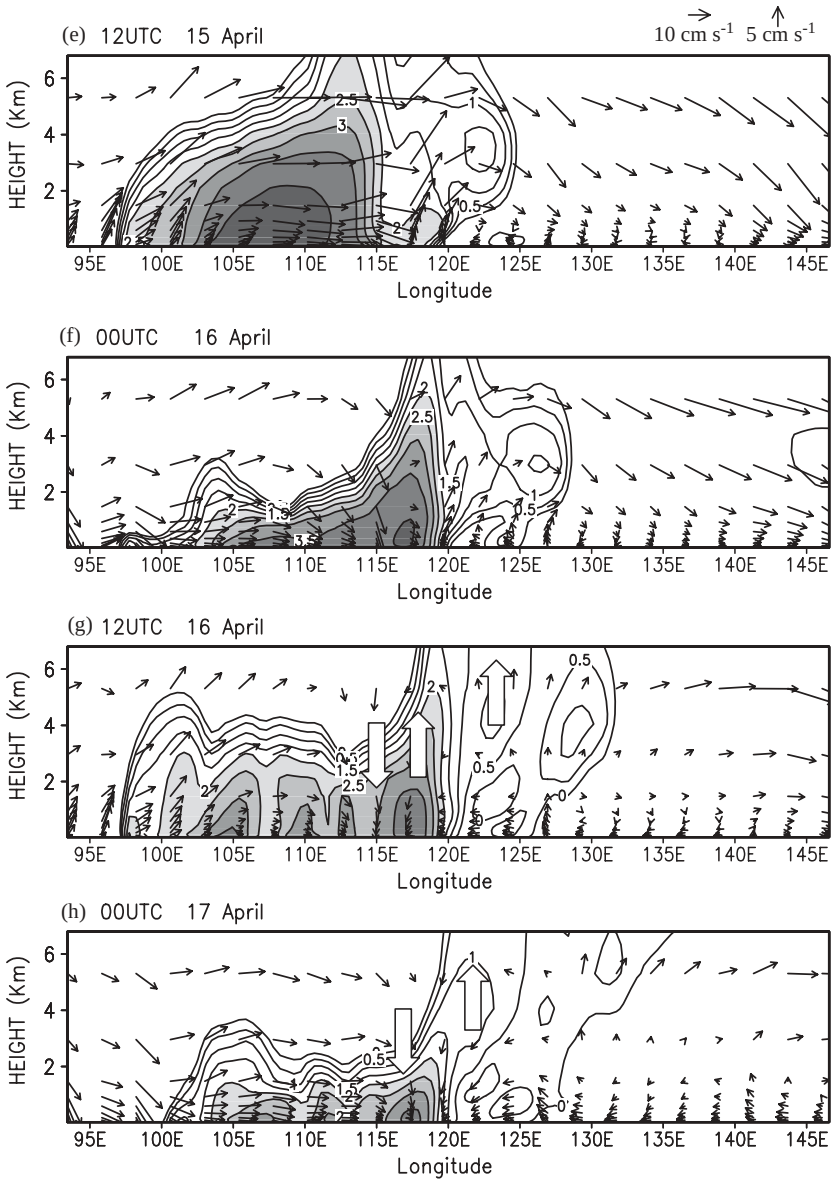

Fig. 6 (*continued*).

of a low pressure center cause dusts to be advected vertically above 8 km height as seen in Beijing, Seoul, and Tokyo (Fig. 7b–d). After the passage of the low-pressure system downward motions confine dusts in the lower layer thereby increasing the ground level concentration. Sometimes upper level dusts just pass by without touching the ground, in which case the ground level concentration is not affected by the dust transport. This is the case in Seoul and Tokyo (Fig. 7c and d). Dusts are mainly confined at the height of 2 km that is similar to other studies (Iwasaka et al., 1983).

4.4. Temporal variations of dust concentrations at several locations

Fig. 8 shows the time series of modeled TSP concentrations averaged for the layers of below 100, 100–1000 and 1000–3000 m above the ground with precipitation amounts at several locations. The estimated emission rate at the Gobi site and Beijing whereas the observed TSP concentration in Seoul and Tokyo are also shown in Fig. 8. The concentrations are generally very low when precipitation occurs. Among sites, the Gobi and Beijing site belong to the source regions (the

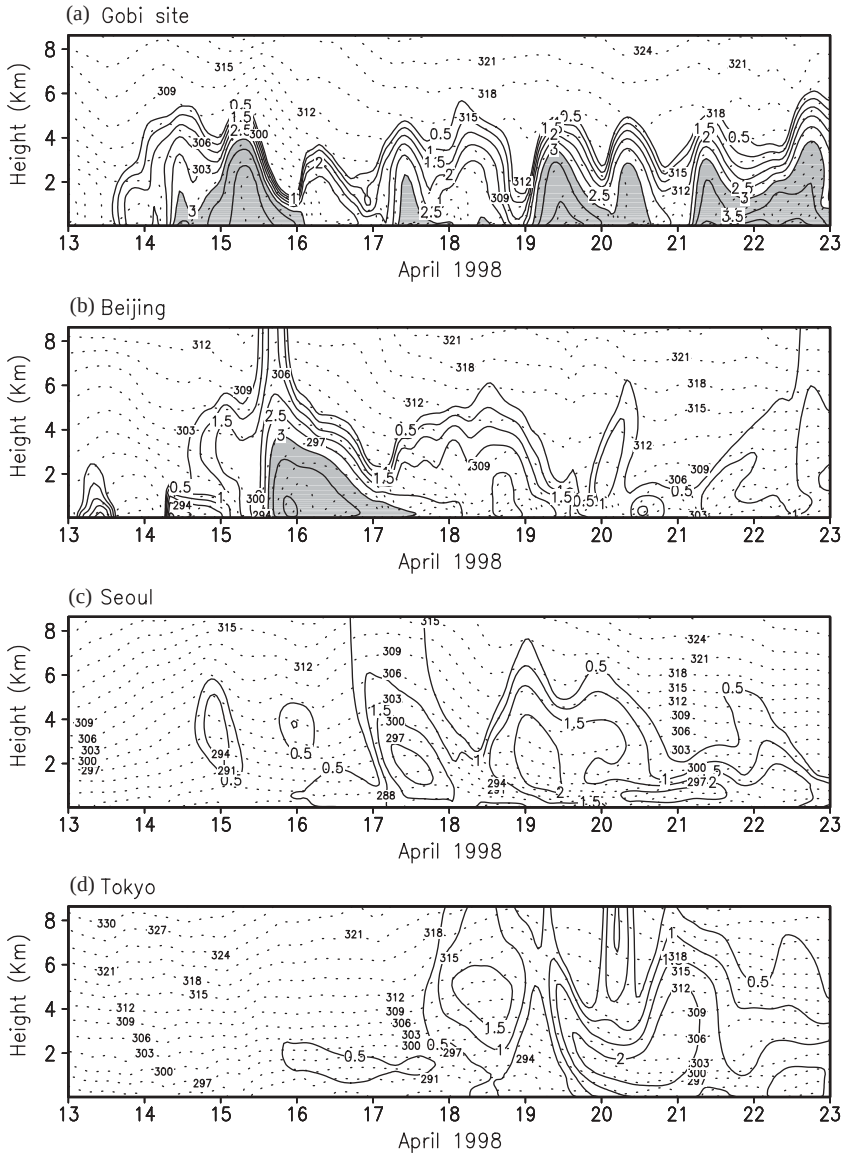

Fig. 7. The time-height cross sections of dust concentration (—, power of 10 μg m^{-3}) and the potential temperature (----, K) at (a) the Gobi site, (b) Beijing, (c) Seoul, and (d) Tokyo for the period of 00 UTC 13 to 00 UTC 23 April.

Gobi site belongs to the Gobi region while Beijing to the Loess region) and are affected by the dust emission directly. Therefore, the TSP concentration extremely depends on dust emission. Seoul and Tokyo are located far away from the source regions, therefore, affected by long-range transport.

When the dust rises in the source region the concentrations increase rapidly reaching to more than 20,000 μg m^{-3} at the Gobi site and the evolution pattern of the concentration in the lowest layer of below 100 m is quite similar to the emission rate (Fig. 8a). The concentration in the lower layer is higher than in the upper layer at this site. In Beijing (Fig. 8b), the dust emissions occur on 13 and 14 April. The ground level dust concentration (the lowest layer) is about 3000 μg m^{-3} with much lower upper level concentration during the emission period on 14 April. On 16 April the ground level concentration shows the maximum value of more than 10,000 μg m^{-3} that is probably caused by advection from other source regions. The upper level concentration in the layer of 100–1000 m reaches its maximum value of 8000 μg m^{-3} at that time.

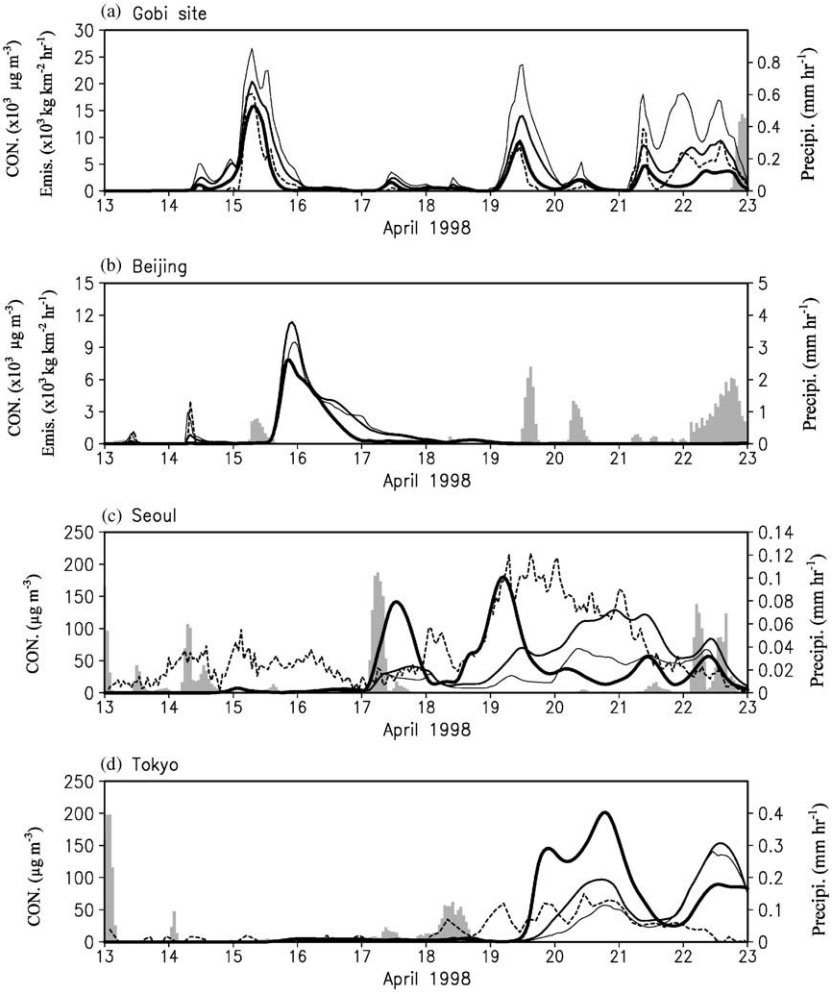

Fig. 8. The time series of modeled mean dust concentration ($\mu g\,m^{-3}$) averaged for the layers of surface to 100 m (—), 100–1000 m (—), and 1000–3000 m (▬) with precipitation rate ($mm\,h^{-1}$) at (a) Gobi site, (b) Beijing, (c) Seoul, and (d) Tokyo. Emission rates ($10^3\,kg\,km^{-2}\,h^{-1}$) at the Gobi site and Beijing and the observed TSP concentrations (----) at Seoul and Tokyo are also shown.

The modeled concentration at Seoul is compared with the observed dust concentrations averaged over the same grid (Fig. 8c). From the TSP concentration observation in Seoul (Fig. 4a), the daily mean concentration in 13 April (one day before Yellow Sand report) is about $50\,\mu g\,m^{-3}$. Thus this value is regarded as the background TSP concentration in Seoul during the Yellow Sand event. The observed concentrations are subtracted by a background value to show the increment due to dust transport. Both modeled ground level concentration and observed one do not increase for the first 4 days and then start to increase from 17 April. The maximum ground level concentration in the model occurs on 20–21 April with a peak value of $70\,\mu g\,m^{-3}$. The average concentration in the layer of 100–1000 m shows a peak value of $120\,\mu g\,m^{-3}$ at 00 UTC 21 April. Thereafter, the concentrations decrease to the background value at the end of event. However the observed concentration in Seoul has a maximum value about $200\,\mu g\,m^{-3}$ on 19 April. This maximum concentration keeps to remain for 1 day. On the other hand, the modeled upper level concentration (1000–3000 m layer) shows a peak at 12 UTC 17 April and 00 UTC 19 April with the value of 140 and $170\,\mu g\,m^{-3}$, respectively. The concentration in the upper level increases earlier than that in the lower layer and the concentration is much higher. The model simulates quite well the starting and ending times of the Yellow Sand event observed in Korea. However, the occurring time of maximum concentration and its value in the model show somewhat

difference with observations. This deviation may be attributed to the discrepancies in dust emissions and simulated meteorological fields. In Tokyo, the estimated lower level TSP concentration is similar to observation except for another peak after 22 April in the model (Uno et al., 2001).

The occurring time of a peak upper-level concentration from the Gobi site (10UTC 15 April) to Beijing (21UTC 15 April) and Seoul (12UTC 17 April) lags by half to 2 days. It denotes the time scale of movement of the dust storm occurred on 15 April in the Gobi region (Fig 8). The leading edge of the dust layer moves southeastward and then turns cyclonically due to a cyclonic vortex. After the dust layer passes over Southeast China, it approaches to Korea and then moves to eastward along 30°N latitude without affecting Tokyo (Fig. 8). The peak concentration in Seoul at 06 UTC 19 April is due to the other dust layer from the north. This dust layer is transported to Tokyo resulting in a maximum concentration on 20 April.

4.5. Particle size distributions

Fig. 9 shows the daily mean dust concentrations of 10 different size bins at 4 different levels (σ value of 0.998, 0.92, 0.80, and 0.55) on the day when the maximum concentration is simulated (Gobi site: 15 April, Beijing: 16 April, Seoul: 19 April, Tokyo: 20 April). The concentration at the Gobi site (Fig. 9a) increases exponentially with particle size because emission fluxes follow the power law. The concentrations in the source region are highly dependent on emission fluxes. However, the concentration of bin 10 is lower than that of bin 9 due to large deposition velocity at $\sigma = 0.92$ (550 m above the ground), and $\sigma = 0.80$ (1400 m above the ground). The concentration distribution at $\sigma = 0.55$ (4900 m height), are somewhat different. Larger particles than bin 8 tend to retain in the lower layer within 4 km above the ground. This makes a uni-modal distribution with a peak at bins 8 and 9 at the $\sigma = 0.55$ level. In Beijing (Fig. 9b), the distributions of particle size are

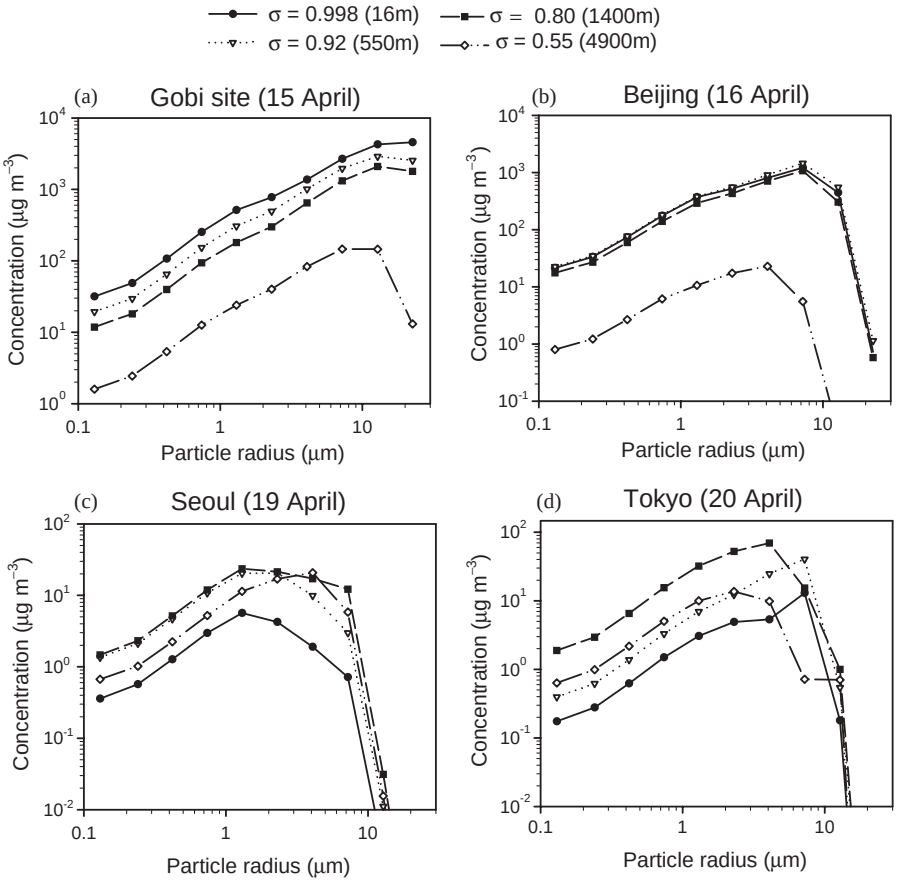

Fig. 9. Distributions of the daily mean dust concentration ($\mu g\,m^{-3}$) with the particle size at $\sigma = 0.998$ (16 m), 0.92 (550 m), 0.80 (1400 m), and 0.55 (4900 m) levels at (a) Gobi site on 15 April, (b) Beijing on 16 April, (c) Seoul on 19 April, and (d) Tokyo on 20 April.

similar to that in the Gobi site except for much lower concentrations of bins 9 and 10.

Usually, far away from the source region the concentrations of large particle size bins become lower. The size distribution in Seoul and Tokyo (Fig. 9c and d) shows the similar patterns having one peak concentration. However, the particle size of maximum concentration is larger in Tokyo. This is attributed to the different origin and pathway of the dust storm. The dust layer located in Manchuria on 18 April (Fig. 5) moves through Tokyo to the East Sea. This dust layer causes a high concentration of large particle in Tokyo on 20 April. In Seoul, the concentration of bins 5–6 at the ground level ($\sigma = 0.998$) is higher in consistent with the observation during spring (March–May) in 1998. The concentration of particles of 2.23–6.06 μm in diameter which corresponds to bins 5 and 6, increases dominantly during the Yellow Sand event in Korea (METRI, 1998). However, in the level of $\sigma = 0.80$ and 0.55 the concentration of bins 6–8 shows high concentration. The ground level ($\sigma = 0.998$) concentration decreases with the increase of bin due to increased dry deposition velocity.

5. Summary and conclusion

Long-range transport of Yellow Sand observed in Korea for the period of 14–22 April in 1998 was simulated using the three dimensional eulerian air quality model with MM5 meteorological outputs together with the physical processes of dust emission, eddy diffusion, transport, dry and wet deposition.

There were large dust rises in 15 and 19 April in the source regions of inland China. The dusts emitted in source regions were advected vertically due to upward motion and large vertical eddy diffusivities and then they transported southeastward following the wind fields. The dust layers emitted on 15 and 19 April had different pathways. On 15–18 April, the dust laden air in southern China moves southward turning counterclockwisely in association with a low pressure vortex and then moved to South Korea and southern Japan. On the other hand, a dust storm developed in northern China on 19 April moved continuously eastward along 45°N latitude line until 22 April. After 20 April the dust laden air over the Korean Peninsula and Japan moves northward due to prevailing southerly winds. The spatial distribution of vertically integrated dust concentration in the model was quite well coincided with that of aerosol index obtained by TOMS. And also the arriving time of the dust storm to the Korean Peninsula was quite well simulated. However, the simulated dust concentration was slightly underestimated the observed TSP concentration in South Korea.

The simulated particle sizes in Korea were found to be less than 6–7 μm in diameter with a uni-modal size distribution at a peak in the range of 1.73–4.03 μm during the Yellow Sand event. These findings were well coincided with observations, suggesting the usefulness of the present model in forecasting the dust storm and the quantitative estimation of dust concentration.

Acknowledgements

This research is partially supported by the Ministry of Education under the Brain Korea 21 Program and Climate Environment System Research Center that is funded by Korea Science and Engineering Foundation. The authors are very grateful two anonymous reviewers for their helpful comments.

References

Bott, A., 1989. A positive definite advection scheme obtained by nonlinear renormalization of the advective fluxes. Monthly Weather review 117, 1006–1015.

Businger, J.A., Wybgaard, J.C., Izumi, Y., Bradley, E.F., 1971. Flux profile relationships in the atmospheric surface layer. Journal of Atmospheric Science 28, 181–189.

Chang, J.S., Brost, R.A., Isaksen, I.S.A., Madronich, S., Middleton, P., Stockwell, W.R., Walcek, C.J., 1987. A three-dimensional Eulerian acid deposition model: physical concepts and formulation. Journal of Geophysical Research 92, 14681–14700.

Chang, J.S., et al., 1991. The regional acid deposition model and engineering model, NAPAP Report 4, National Acid Precipitation Assessment Program, Washinton, DC.

Chun, Y.-S., 1966. Long-range transport of Yellow Sand with special emphasis on the dust rise conditions in the source regions. Ph.D. dissertation. Department of Atmospheric Sciences, Seoul National University, pp. 30–45 (Korean).

Chun, Y., Kim, J., Choi, J.C., Boo, K.O., Oh, S.N., Lee, M., 2001. Characteristic number size distribution of aerosol during Asian dust period in Korea. Atmospheric Environment 35, 2715–2721.

Chung, K.-Y., 1996. Numerical simulations of Yellow Sand events observed in Korea. Ph.D. dissertation. Department of Atmospheric Sciences, Seoul National University, pp. 47–54 (Korean).

Dudhia, J., Gill, D., Guo, Y.-R., Hansen, D., Manning, K., Wang, W., 1998. PSU/NCAR mesoscale modeling system tutorial class notes (MM5 modeling system version 2).

Gillette, D.A., 1981. Special Paper Geological Society of America 186, 11–26.

Grell, G.A., Dudhia, J., Stauffer, D.R., 1994. A description of the fifth-generation Penn State/NCAR mesoscale mode (MM5). NCAR TECH. Note NCAR/TN-398+STR, 117pp.

Hanna, A.F., Mathur, R., Alapathy, K., Pinto, J., 1999. Modeling the episode transport of air pollutants from Asia to North America. http://Envpro.ncsc.org/projects/MITP.

Husar, R.B., Tratt, D.M., Schichtel, B.A., Falke, S.R., Li, F., Jaffe, D., Gasso, S., Gill, T., Laulainen, N.S., Lu, F., Reheis, M.C., Chun, Y., Westphal, D., Holben, B.N., Gueymard, C., McKendry, I., Kuring, N., Feldman, G.C., McClain, C., Frouin, R.J., Merrill, J., DuBois, D., Vignola, F., Murayama, T., Nickovic, S., Wilxon, W.E., Sassen, K., Sugimoto, N., 2001. The Asian dust events of April 1998. Journal of Geophysical Research 106, 18317–18330.

In, H.-J., Park, S.-U., 2002. Estimation of dust emission amounts for a dust storm event occurred on April 1998 in China. Water, Air and Soil Pollution, In press.

Iwasaka, Y., Minpoura, H., Nagata, K., 1983. The transport and spatial scale of Asian dust storm clouds: a case study of the dust storm event of April 1979. Tellus 35B, 189–196.

Keyser, D., Carlson, T.N., 1984. Transverse ageostrophic circulations associated with the elevated mixed layer. Monthly Weather Review 112, 2465–2478.

Lanicci, J.M., Warner, T.T., 1991. A synoptic climatology of the elevated mixed layer inversion over the southern great plains in spring. Part 1: structure, dynamics and seasonal evolution. Weather Forecasting 6 (2), 181–197.

Meteorological Research Institute/Korea Meteorological Administration, 1998. Intensive Observation and Analysis of Aerosol in spring in Seoul.

Park, S.-U., Chang, L.-S., 2000. A numerical simulation of a Yellow Sand event observed in Korea during 14–23 April. Proceedings of Trans-Pacific Conference, Washington, USA.

Schûtz, L., Jaenicke, R., 1974. Journal of Applied Meteorology 13, 863–870.

Stensrud, D.J., 1993. Elevated residual layers and their influence on surface boundary layer evolution. Journal of Atmospheric Sciences 50 (14), 2284–2293.

Uno, I., Amano, H., Emori, S., Kinoshita, K., Matsui, I., Sugimoto, N., 2001. Trans-Pacific Yellow Sand transport observed in April 1998. Journal of Geophysical Research 106, 18331–18344.

Wesely, M.L., 1989. Parameterization of surface resistance to gaseous dry deposition in regional-scale numerical models. Atmospheric Environment 23, 1293–1304.

Wesely, M.L., Cook, D.R., Hart, R.L., Speer, R.E., 1985. Measurements and parameterization of particulate sulfur dry deposition over grass. Journal of Geophysical Research 90, 2131–2143.

Westphal, D.L., Toon, O.B., Carlson, T.N., 1987. A two-dimensional investigation of the dynamics and microphysics of Saharan dust storms. Journal of Geophysical Research 92, 3027–3049.

Westphal, D.L., Toon, O.B., Carlson, T.N., 1988. A case study of mobilization and transport of Saharan dust. Journal of Atmospheric Sciences 45, 2145–2175.

Yoon, S.-C., Won, J.-K., 1998. Measurement of Yellow Sand using LIDAR. Proceedings of Conference of Korean Meteorological Society, 235–237 (Korean).

Zhang, Y., Carmichael, G.R., 1999. The role of mineral aerosol in tropospheric chemistry in East Asia—a model study. Journal of Applied Meteorology 38, 353–366.